

# Mechanics of Leukocyte Deformation and Adhesion to Endothelium in Shear Flow

CHENG DONG, JIAN CAO, ERIKA J. STRUBLE, and HERBERT H. LIPOWSKY

Bioengineering Program, The Pennsylvania State University, University Park, PA

(Received 10 February 1998; accepted 28 April 1998)

**Abstract**—The mechanics of leukocyte [white blood cell (WBC)] deformation and adhesion to endothelial cells (EC) in shear flow has been investigated. Experimental data on transient WBC–EC adhesion were obtained from *in vivo* measurements. Microscopic images of WBC–EC contact during incipient WBC rolling revealed that for a given wall shear stress, the contact area increases with time as new bonds are formed at the leading edge, and then decreases with time as the trailing edge of the WBC membrane peels away from the EC. A two-dimensional model (2D) was developed consisting of an elastic ring adhered to a surface under fluid stresses. This ring represents an actin-rich WBC cortical layer and contains an incompressible fluid as the cell interior. All molecular bonds are modeled as elastic springs distributed in the WBC–EC contact region. Variations of the proportionality between wall shear stress ( $\tau_w$ ) in the vicinity of the WBC and the resulting drag force ( $F_s$ ), i.e.,  $F_s/\tau_w$ , reveal its decrease with WBC deformation and increasing vessel channel height (2D). The computations also find that the peeling zone between adherent WBC and EC may account for less than 5% of the total contact interface. Computational studies describe the WBC–EC adhesion and the extent of WBC deformation during the adhesive process. © 1999 Biomedical Engineering Society. [S0090-6964(99)01103-0]

**Keywords**—*In vivo*, Incipient cell rolling, Transient contact, Drag force, Modeling.

## INTRODUCTION

Leukocyte [white blood cell (WBC)] adhesion to endothelial cells (EC) of postcapillary venules is a fundamental step in the inflammatory process which precedes their emigration through the microvessel wall. It is generally recognized that firm adhesion is the final result of a sequence of dynamic events that begins with the radical migration of WBCs to the venular wall, its subsequent rolling along the EC, and finally WBC arrest and attachment to the EC.<sup>24</sup> The process of WBC adhesion and rolling involves a complex balance of forces arising from hydrodynamic shearing effects and the strength of the adhesive bond between the WBC and EC. This bal-

ance depends strongly on WBC deformability<sup>14</sup> and the expression of adhesion receptors and ligands.<sup>19,24</sup>

For example, observations of WBC rolling *in vivo* have shown that as the blood wall shear rate ( $\dot{\gamma}$ ) increases from 50 to 800  $\text{s}^{-1}$ , WBCs elongate to 140% of their undeformed diameter, and the contact area between WBC and substrate increases 3.6-fold.<sup>14</sup> These data emphasize the potential of cell-shape changes with deformation to affect WBC rolling and adhesion by either alteration of the resistance to deformation or the strength of the adhesive WBC–EC bonds. For example, the velocity of WBC rolling in venules was found to vary very little at all shear rates, thus suggesting that the greater deformation of WBCs rolling at high shear rates results in greater adhesive forces that attenuate further increases of WBC rolling velocity as shear stress is increased. Also, the stretching and elongation of the WBC in shear flow may help temper hemodynamic drag forces on the WBC by reducing the extent of the vessel lumen obstructed by the WBC.<sup>18</sup>

Significant progress has been made in the past decade toward understanding the receptor-mediated cell adhesion which is involved in the WBC–EC interaction. Detailed experimental studies of the adhesive bonds have suggested that adhesion molecules of the selectin family are involved in maintaining the initial rolling of leukocytes on the endothelium, whereas the much stronger integrin bonds are responsible for firm and prolonged WBC attachment to the EC.<sup>19,24</sup>

Analysis of the forces involved in WBC–EC adhesion at the equilibrium state was pioneered by Bell.<sup>3</sup> Based upon Zhurkov's<sup>30</sup> kinetic theory of fracture, the analysis of the separation of two cells firmly adhered to one another was cast in terms of the thermodynamics of bond separation. Evans<sup>11</sup> established a theoretical framework of a one-dimensional tape-peeling model to compute the adhesion force between a biomembrane and a substrate with constant adhesive strength. To study the receptor-mediated cell adhesion to a ligand-coated surface, Hammer and Lauffenburger<sup>17</sup> took steps from Bell's theory<sup>3</sup> and developed a cell adhesion model taking receptor–

Address correspondence to C. Dong, Bioengineering Program, 229 Hallowell Building, Penn State University, University Park, PA 16802. Electronic mail: cxd23@psu.edu

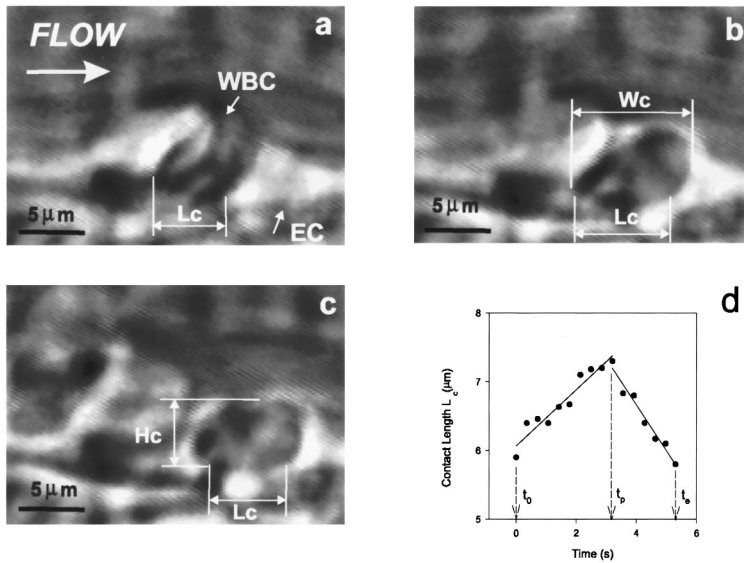


**FIGURE 1.** *In vivo* video images of a rat's leukocyte (WBC) adhering to the venular endothelium (EC) characterized by the WBC–EC contact length  $L_c$  at various times in the blood flow. Wall shear stress =  $7.7 \text{ dyn/cm}^2$ . (a) WBC just adheres to the EC at time  $t = t_0$  (0 s). (b) WBC reaches its largest deformation at time  $t = t_p$  (3.2 s). (c) WBC peels away from the EC at time  $t = t_e$  (5.3 s). (d) Representative measurements on  $L_c$  changing as a function of time.

ligand bond kinetics into consideration. By considering the influence of the mechanical properties of the cell membrane, Dembo and co-workers<sup>5</sup> extended Evans' tape-peeling theory by adding receptor–ligand bond kinetics into their model and computed the adhesion force between a cell membrane and its adherent substrate. With a similar approach, Ward *et al.*<sup>27</sup> further explored the effect of ligand density on the detachment of the cell membrane from a substrate. While other simple geometric models have been previously used to represent cell-to-surface adhesion,<sup>1,15,17,26</sup> no previous study has elucidated the mechanics of shape change for the entire cell due to deformation and adhesion under shear flow conditions. It is thus evident that greater insight is needed on the mechanisms that determine how hydrodynamic forces acting on the cell surface are transmitted, via cell deformation, into forces which disrupt individual receptor–ligand bonds between the WBC and EC.

To explore the role of WBC deformation in the process of WBC–EC adhesion, the present study has aimed to develop a biomechanical model using the theory of an elastic thin shell coupled with adhesion bond kinetics. The model includes a two-dimensional cell-shape change due to deformation and determines the relationship between cell membrane mechanics and the receptor-mediated WBC–EC adhesion. A finite-element computational model was used to calculate the hydrodynamic force and torque exerted on individual cells in a shear flow. The equilibrium among forces arising from hydrodynamic shearing effects due to the blood flow, and the strength of the adhesive receptor–ligand bonds between WBC and EC is considered. Results show that both the net hydrodynamic force and adhesion force are influenced by both the cell deformability and cell–surface adhesion kinetics. Comparison of the model with *in vivo*

data indicates that WBC deformability is an essential component that aids in the adhesion process to balance the hemodynamic and WBC–EC adhesive forces.

## EXPERIMENTAL OBSERVATIONS

To assess the relationship between cell membrane mechanics and the formation and disruption of WBC–EC adhesion bonds, both the WBC–EC contact area and WBC shape have been studied using *in vivo* experiments during incipient WBC attachment and detachment to the EC.<sup>25</sup> Briefly, a high-magnification water immersion objective ( $\times 40$ ) was used to record the transient adhesion of WBCs to the lateral edges of postcapillary venules in mesentery (rats), as described by Lipowsky *et al.*<sup>21</sup> The wall shear stress due to the flow was estimated as the Newtonian value of  $8\mu V_{\text{mean}}/D$ , where  $D$  denotes vessel diameter,  $V_{\text{mean}}$  represents the mean-blood velocity, and  $\mu$  is the blood viscosity (an average value of blood viscosity of 0.025 P was assumed).  $V_{\text{mean}}$  was estimated from the red cell [red blood cell (RBC)] velocity  $V_{\text{RBC}}$ , obtained along the center line of the vessel by the empirical relationship for the video two-slit photometric technique  $V_{\text{mean}} = V_{\text{RBC}}/1.6$ .<sup>2</sup> Images of WBC adhesion to, and detachment from the EC were recorded on video tape for subsequent analyses. WBC-shape changes and alterations in the contact length between the WBC and EC during the transient adhesion were characterized.

The recorded video images of WBC–EC adhesion were used as a reference guide for development of the computational cell model. For an illustration, three representative shapes of a WBC transiently adhering to the EC are shown in Fig. 1. The cell shape shown in Fig. 1(a) represents a WBC that has just adhered to the surface of the EC, prior to deforming in response to a wall

shear stress ( $\tau_w$ ) of 7.7 dyn/cm<sup>2</sup>. It has been noticed that the cell is deformed from its original circular shape to a teardrop shape along the direction of flow in the blood stream prior to cell attachment. Following the attachment, the cell deforms with time due to the elongation of the cell membrane and deformation of the cell body under the influence of hydrodynamic and adhesion forces. Also, the WBC–EC contact length ( $L_c$ ) [Fig. 1(a)] steadily increases with time as new bonds are formed at the leading edge of the WBC membrane. The starting time of the WBC deformation was defined as  $t_0$  ( $t_0=0$  s), which is the time of initial attachment to the EC. When the WBC adheres to the EC for about 3.2 s, the cell becomes most deformed as evidenced by having the largest projection length ( $W_c$ ) and  $L_c$  [Fig. 1(b)]. The corresponding time for a cell to reach its largest deformation was denoted as  $t_p$ , which is the time that the WBC starts to be peeled away from the EC. Eventually, the WBC is detached from the EC after 5.3 s which was defined as the ending time ( $t_e$ ) [Fig. 1(c)]. During this period,  $L_c$  subsequently decreases with time as the trailing edge of the WBC membrane is peeled away from the EC during initiation of cell detachment. Frame-by-frame analysis of video recordings facilitated the measurement of  $L_c$ ,  $W_c$ , and height ( $H_c$ ) as shown in Figs. 1(a), 1(b), and 1(c), respectively. Linear regressions of  $L_c$  versus time were used to characterize the relationship among cell dimensions ( $H_c$ ,  $W_c$ , and  $L_c$ ) and wall shear stress  $\tau_w$  for two distinct time periods:  $t_0 \leq t \leq t_p$  and  $t_p \leq t \leq t_e$ , as illustrated in Fig. 1(d) for this representative cell. Since the  $H_c$  and  $W_c$  could be easily measured from the *in vivo* images, we therefore used the  $H_c/W_c$  ratio as a key index to validate the cell model, and a comparison between the computed and measured values of  $L_c$  could be obtained.

## THEORETICAL FORMULATIONS

A theoretical model of *in vivo* WBC–EC adhesion was developed. Using a two-dimensional (2D) approximation to the actual three-dimensional (3D) cell body, a cross-sectional slice of an adherent WBC was formulated, which was made by the cell membrane through the azimuth center of the cell [Fig. 2(a)]. The cell was represented by a 2D extensible elastic ring adhered to a plane surface with steady-state fluid stress and adhesive contact stress as they were acting to deform the WBC *in vivo*. In actuality, this ring may represent an actin-rich cortical layer under the WBC surface. The model also included the kinetics of adhesion bond formation and disruption within the WBC–EC contact region. All molecular bonds were modeled as elastic springs, which were distributed in the contact region to generate the contact stress to the adherent ring. To determine the

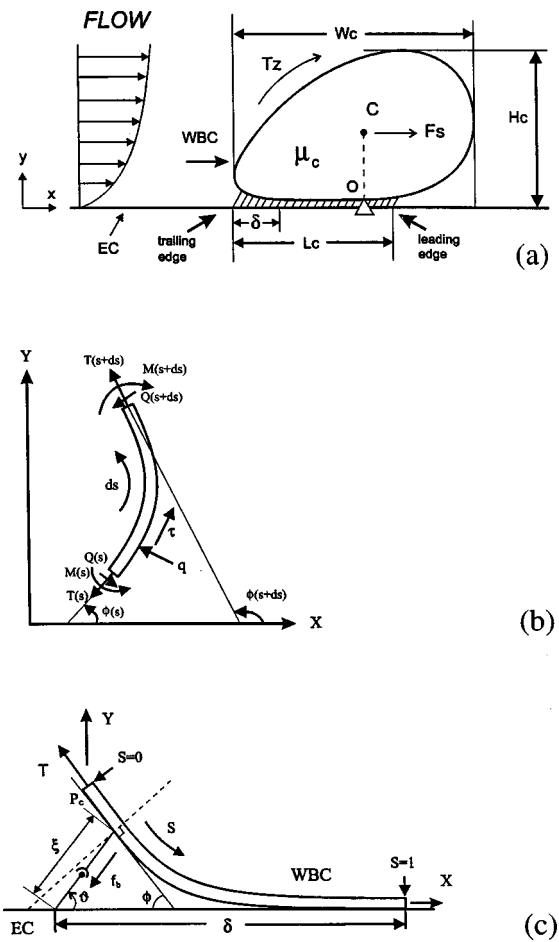


**FIGURE 2.** (a) Schematic drawing of a 2D cell adhesion model.  $H_c$  is the height;  $W_c$  is the projection length;  $L_c$  is the contact length;  $\delta$  is the active peeling zone;  $\mu_c$  is the intracellular viscosity;  $\phi$  is the angle between a tangent drawn from a point on the ring surface to the substrate;  $F_s$  is the fluid drag force; and  $T_z$  is the torque with respect to the point O (the projection point of mass center C). (b) A segment of the cell cortical layer modeled by an elastic ring.  $Q$ ,  $T$ , and  $M$  are the transverse shear, membrane tension, and bending moment, respectively.  $q$  and  $\tau$  are the total normal and tangential surface stresses, respectively.  $s$  is the surface coordinate. (c) Schematic illustration of an adhesion bond in the region of WBC–EC contact. Each individual bond is modeled by an elastic spring with a tilted angle  $\theta$  to the substrate.  $\xi$  is the stretch length of the bond.  $T$  is the membrane peeling tension and  $\delta$  is the active peeling zone.

shape of a deformed cell, static equilibrium between hydrodynamic shear stress and adhesive force was considered as follows.

### *An Extensible Elastic Ring Adhered to A Plane Surface in Shear Flow*

The undeformed shape of the elastic ring was assumed to be circular with radius  $R_c$ . When the cell is subjected to a steady fluid stress, the elastic ring deforms to a teardrop-like configuration [Fig. 2(a)]. The effect of

cell membrane folds or wrinkles, which provide about 80%–100% excess area over that needed to envelope the cell volume by a smooth spherical surface (undeformed WBC), was characterized by the extensibility of the elastic ring in terms of its surface stretch ratio ( $\lambda$ ). The WBC–EC contact area was characterized by the contact length  $L_c$  in the 2D model. The cell interior was assumed to be an incompressible, viscous Newtonian fluid under the quasistatic state with a viscosity of  $\mu_c$ . For a 2D case, the cell volume incompressibility in 3D was then approximated by an area conservation that the ring enclosed. The membrane elasticity and cytoplasmic viscosity will determine the degree of cell deformation. Formulation of the membrane mechanics was developed along the cell surface for nonadherent and adherent regions as follows.

In the nonadherent region, it was assumed that the external stresses from the steady shear flow had a normal component  $q_f$  and a tangential component  $\tau_f$  on the cell surface, respectively, as shown in Fig. 2(b). Prior studies of WBC deformation suggested that a simple membrane theory might be adequate to describe the rheological behavior of the WBC cortical layer by neglecting the bending properties.<sup>7,8,13</sup> In a recent study, Zhelev *et al.*<sup>29</sup> included the bending stiffness to model the WBC cortical layer and cell deformation. In the present analysis, the WBC cortical layer has included the effect of both bending stiffness and surface folds during cell deformation in a shear flow:

$$Q' - kT - q = 0, \quad (1)$$

$$T' + kQ + \tau = 0, \quad (2)$$

$$M' - Q = 0. \quad (3)$$

Equations (1)–(3) govern the equilibrium of the ring segment as shown in Fig. 2(b).  $Q$ ,  $T$ , and  $M$  are the transverse shear, the tension, and the bending moment, respectively;  $q$  and  $\tau$  are the total normal and tangential surface stresses, respectively. The prime (') indicates the differential  $d/ds$ , in which  $s$  is the surface coordinate along the midsurface starting at the leading edge of the ring–substrate contact point and going counterclockwise. The bending moment  $M$  can be assumed to be

$$M = \lambda B(k - k_0), \quad (4)$$

where  $B$  is the bending stiffness of the cortical layer;<sup>12</sup> and  $k$  is the curvature of the ring that is equal to  $\phi'(s)$ , where  $\phi(s)$  is the angle between a tangent drawn from a point on the surface of the ring to the  $x$  axis.  $k_0$  is the reference curvature of the ring in the resting (undeformed) state.  $\lambda$  is the stretch ratio of the ring along the

circumference in the direction of the flow, which should reflect the properties of the leukocyte cortical layer in terms of the membrane surface folds [Fig. 2(b)].

For a 2D model, the width of the ring may be assumed to be constant during cell deformation, so that the cell surface area change is approximated by  $\Delta A/A = \lambda - 1$ . If  $T_0$  is assumed to be the prestressed tension in the cortical layer, the stretch ratio in Eq. (4) can be expressed by the approximation<sup>9</sup>

$$\lambda = 1 + \sqrt[n]{\frac{T - T_0}{E}} \quad \text{or} \quad T = T_0 + E(\lambda - 1)^n, \quad (5)$$

where  $E$  is the elastic modulus for the membrane surface area dilatation and  $n$  is a positive finite number ( $E = 0.15$  dyn/cm,  $n = 1$  were used by Dong and Skalak<sup>9</sup>). From Eqs. (1)–(4), one obtains a single fourth-order nonlinear ordinary differential equation for  $\phi(s)$ , together with Eq. (5), which describes the deformation of the upper surface of the cell (Fig. 1), i.e.,

$$\begin{aligned} & \frac{B\phi''''}{\phi'} - \frac{q'}{\phi'} - \frac{\lambda B\phi''\phi'''}{(\phi')^2} + \frac{\phi''q}{(\phi')^2} + \lambda B\phi'\phi'' + \tau \\ & + \lambda''B\left(1 - \frac{k_0}{\phi'}\right) + \frac{2\lambda''B\phi''}{\phi'} + \frac{3\lambda'B\phi'''}{\phi'} \\ & - \frac{2\lambda'B(\phi'')^2}{(\phi')^2} + \frac{\lambda''B\phi''k_0}{(\phi')^2} + \lambda'B(\phi')^2 = 0. \end{aligned} \quad (6)$$

This equation may be separated into a set of four first-order nonlinear ordinary differential equations and solved by using a Runge–Kutta method (IMSL, Houston, TX) as an initial value problem.

In the adherent region, the mechanical response of the cell membrane to the WBC–EC adhesion was formulated. All adhesion bonds within the adherent region were assumed to be oriented at an angle ( $\theta$ ) to the substrate [Fig. 2(c)], with a force  $f_b$  from each receptor–ligand bond. The strength of the adhesive bonds to resist all horizontal forces from the shear flow  $F_s$  was determined by integration of the product of an individual bond force  $f_x$  (the sum of the horizontal component of  $f_b$ ) and a bond density  $N_b$  over the entire contact area  $A_c$  in the direction of flow [Fig. 2(a)]. It is hypothesized in the present model that only those bonds in the active peeling region ( $\delta$ ) near the trailing edge [Figs. 2(a) and 2(c)], rather than the entire contact region ( $L_c$ ), would be stretched during the cell membrane peeling process and, therefore, resist  $F_s$  on the cell. In the region beyond the  $\delta$  zone within  $L_c$ , all bonds were assumed to be compressed for a balance of forces in the  $y$  axis. The fluid torque  $T_z$  exerted on the cell body and the torque

generated by the stretched adhesive bonds in the  $\delta$  zone were balanced with respect to the point O [Fig. 2(a)], i.e., the projection point of the mass center C. The torque generated beyond the  $\delta$  zone was neglected, which was believed to be much less than the torque generated from the peeling zone  $\delta$ . The current modeling approach has focused on a very small peeling zone reflected by  $\delta/L_c$ .

In terms of membrane displacement  $Y(s)$  [Fig. 2(c)], the local mechanical equilibrium within the  $\delta$  zone was formulated in a similar way to Eq. (6), by letting  $q = -\sigma_b - q_{in}$ , and  $\tau = \tau_b$ , where  $q_{in}$  is the normal stress of the cell interior; and  $\sigma_b$  and  $\tau_b$  are the normal and shear adhesive-bond stresses, respectively.  $s$  represents the curvilinear coordinate, starting at the trailing edge (point  $P_c$ ;  $s=0$ ) counterclockwise along the ring surface within the peeling zone  $\delta$ .  $X = \delta$  ( $s=1$ ) represents the end point of the peeling zone, at which the membrane surface is tangential to the substrate with zero-bond stretch or compression ( $Y=0$ ).

The formulation of adhesive-bond separation was based on the reaction model developed in the literature,<sup>3,5,17</sup> in which the bond density  $N_b$  may be related to the kinetics of bond formation by

$$\frac{\partial N_b}{\partial t} = V_p \frac{\partial N_b}{\partial s} + K_+(N_l - N_b)(N_r - N_b) - K_- N_b, \quad (7)$$

where  $N_r$  is the initial density of total receptors on the WBC surface and  $N_l$  is the initial density of total ligands on the EC.  $K_+$  and  $K_-$  are the forward and reverse rate constants, respectively, which have been proposed in the following forms:<sup>16</sup>

$$K_+ = K_+^0 \exp\left(-\frac{K_{ts}\xi^2}{2B_z}\right), \quad (8)$$

$$K_- = K_-^0 \exp\left(-\frac{(K_s - K_{ts})\xi^2}{2B_z}\right), \quad (9)$$

where  $B_z$  is the product of the Boltzman constant and temperature;  $K_s$  is the bond elastic constant;  $K_{ts}$  is the transition state bond elastic constant;  $\xi$  is the stretch length of a bond [Fig. 2(c)]; and the superscript ‘‘0’’ refers to the reaction rates at the state of zero stretch of the bonds. In the region beyond the  $\delta$  zone [Fig. 2(a)],  $K_+$  and  $K_-$  were assumed to be constant and equal to  $K_+^0$  and  $K_-^0$ , respectively. The above kinetic equations govern the bond density variation as a function of both space and time within the contact area, including the critical trailing edge where the bond is separated due to the peeling force. A receptor–ligand bond was assumed to be disrupted only if the bond density became below

the critical bond density,  $N_{bc} = 10^{-4} N_{b0}$ .<sup>5</sup>  $N_{b0}$  is the initial bond density solved by

$$0 = K_+^0 (N_l - N_{b0})(N_r - N_{b0}) - K_-^0 N_{b0}. \quad (10)$$

At the contact point  $s = P_c$  [Fig. 2(c)], the bond density  $N_b$  was assumed to be  $N_{b0}$  at time  $t = t_0$  and subsequently dropped to  $N_{bc}$  at time  $t = t_p$  in the present model. For  $s < P_c$ , it was assumed that  $N_b < N_{bc}$  and bond stresses are negligible. Letting  $V_p$  be the peeling velocity given by  $V_p = \partial P_c / \partial t$ ,<sup>5,6</sup> with a reference frame fixed at the moving point  $P_c$ , then  $V_p = 0$  if  $t < t_p$ . For time period  $t \geq t_p$ ,  $V_p$  is given by

$$V_p = \left\{ -[K_+(N_l - N_b)(N_r - N_b) - K_- N_b] \left/ \frac{\partial N_b}{\partial s} \right. \right\} \Big|_{s=P_c}. \quad (11)$$

Therefore, the detachment process requires that the peeling velocity  $V_p > 0$ .

In terms of  $\xi(s)$  [Fig. 2(c)], if one receptor–ligand bond generates a tension force  $f_b$  given by  $f_b = K_s \xi$ , then the normal bond stress  $\sigma_b$  can be expressed by

$$\sigma_b = N_b f_b \sin(\theta + \phi). \quad (12)$$

The adhesive shear stress  $\tau_b$  can also be expressed by

$$\tau_b = -N_b f_b \cos(\theta + \phi). \quad (13)$$

Equations (12) and (13), therefore, provide a bridge between the molecular influence of bond kinetic distribution [Eqs. (7)–(9)] and the continuum model of cell deformation in formulating adhesive-bond stresses  $\sigma_b$  and  $\tau_b$  in the peeling region [Fig. 2(b)].

### Fluid–Solid–Coupled Model

The effects of coupling the moving fluid (blood) and the deformation of an adherent cell were also considered in the present study. Given that shear stresses produced by the blood stream cause a deformation of the cell, the effect of the resultant cell-shape change on the hydrodynamic flow field was estimated by a computational fluid dynamic model of flow over a deformed cell body. The blood was assumed to be a homogenous, incompressible Newtonian fluid with a viscosity of 1.3 cp. The two-dimensional steady-state flow field was calculated using the finite-element method (FIDAP, Evanston, IL) to solve the equations of conservation of mass

$$\nabla \cdot u = 0, \quad (14)$$

and momentum

$$\frac{\partial u}{\partial t} + u \cdot \nabla u = -\nabla p + \frac{1}{\text{Re}} \nabla^2 u, \quad (15)$$

where  $u$  is the velocity vector;  $p$  is the fluid pressure;  $t$  is the time; and  $\text{Re}$  is the Reynolds number based on the radius of the cell.

To minimize the influence of the inlet and outlet boundary conditions, the entrance and exit lengths were chosen to be 8 and 13 times the undeformed cell diameter, respectively. The velocity profile was assumed to be parabolic and unidirectional at the entrance. Additional boundary conditions included no slip and no penetration at the lower and upper wall, no slip condition on the cell surface, and a unidirectional velocity profile without normal stress at the outlet.

Computational grids were generated using the automatic mesh generator in the FIDAP software with a refinement of the grids near the cell surface [Fig. 3(a)]. The sharp corner near the cell–surface contact regions was replaced by a smooth curve to avoid overlap grids. A nonlinear, steady analysis with an initial guess of Stokes flow was specified. The Galerkin method with weighted residuals was used to form integral equations. The penalty function approach was used to replace the pressure variable (i.e.,  $\nabla \cdot u = -\epsilon p$  with  $\epsilon = 10^{-7}$ ), and the integration was achieved by Gaussian quadrature. Grid optimization was achieved by testing the influence of the mesh density on the shear stress and normal stress computations. 2280 element nodes were used to characterize the geometry of capillary venules and the flow field, as shown in Fig. 3(a). The fluid drag force was computed by integrating the shear and normal forces along the cell surface as follows:

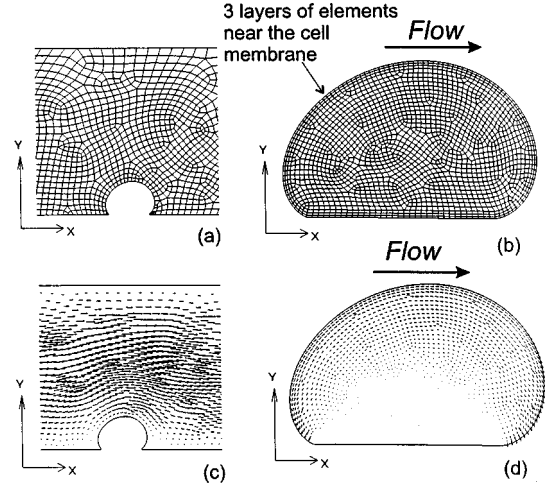


**FIGURE 3.** A typical finite-element grid used for a flow field and an adherent cell generated by FIDAP. (a) and (c): Extracellular flow field containing an adherent cell on the substrate boundary. (b) and (d): Intracellular flow field for a deformable cell under shear.

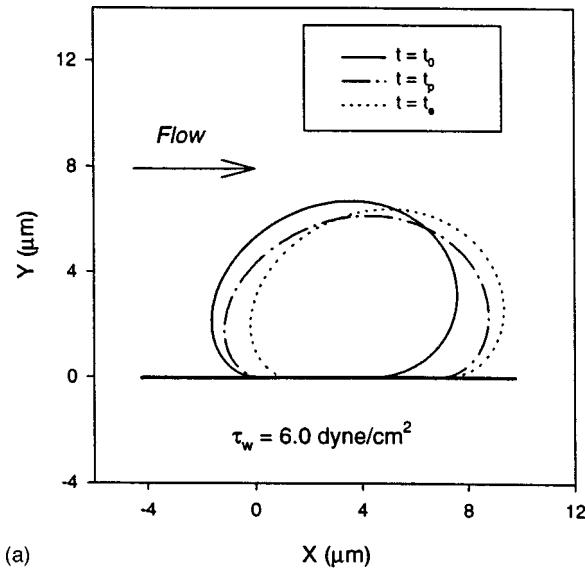
$$F_i = \int_S \sigma_{ij} n_j dS, \quad (16)$$

where  $n_j$  is the unit normal vector on the cell surface  $S$  [Fig. 2(b)]. For a 2D model, the incompressibility of a 3D cell volume was approximated by a conservation of the area enclosed by an elastic ring multiplying the ring width (i.e., a volume  $V = \text{area} \times \text{width} = 4\pi R_c^3/3$  for a cell with a radius of  $R_c$ ). A constant ring width of  $6 \mu\text{m}$  was chosen for the present computation.  $\sigma_{ij}$  is the total stress tensor for the flow field. Knowing the force  $F$ , the fluid torque  $T_z$  with respect to the pivot point  $O$  [Fig. 2(a)] was given by

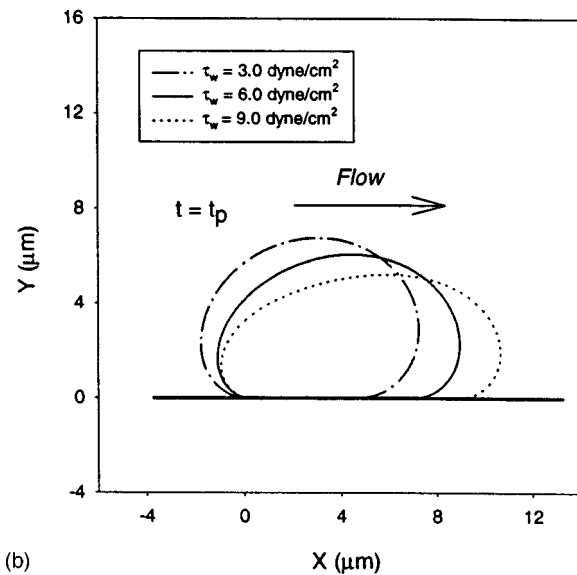
$$T_z = \sum_{k=1}^N F_k \cdot M_k, \quad (17)$$

**TABLE 1.** Parameters used in deformation and adhesion model.

Symbol	Definition	Value	Reference
$R_c$	WBC radius	$4.0 \mu\text{m}$	23
$D$	Venule diameter in rat (average)	$30 \mu\text{m}$	25
$E$	WBC membrane area modulus	$0.12 \text{ dyn/cm}$	9
$B$	WBC membrane bending stiffness	$1.15 \times 10^{-9} \text{ dyn cm}$	29
$N_r$	Total receptor density	$2-5 \times 10^{10} \text{ mol/cm}^2$	19
$N_l$	Total ligand density	$2-5 \times 10^{10} \text{ mol/cm}^2$	19
$K_+^0$	Forward rate constant	$5.5 \times 10^{-11} \text{ cm}^2/\text{s}$	19
$K_-^0$	Reverse rate constant	$1.3 \text{ 1/s}$	3
$K_s$	Bond elastic constant	$4.0 \text{ dyn/cm}$	5, 16
$K_{ts}$	Transition state bond elastic constant	$3.96 \text{ dyn/cm}$	5, 16
$L_b$	Bond length	$50 \text{ nm}$	24



(a)



(b)

**FIGURE 4.** Computed 2D shapes of a WBC adherent to the EC in a shear flow. Model parameters used for computations are listed in Table 1. (a) An undeformed cell shape was assumed to be a circular ring that touches the substrate at time  $t=0$  s. At time  $t=t_0$  ( $0^+$  s), this ring quickly deforms into a teardrop (solid line) forming an initial contact length  $L_c$  as shown in Fig. 1(a). Time  $t_p$  is the instant at which the cell undergoes the largest deformation. Wall shear stress =  $6.0 \text{ dyn/cm}^2$ . (b) Deformed cell shapes at time  $t=t_p$  with different shear stresses of 3.0, 6.0, and  $9.0 \text{ dyn/cm}^2$ .

where  $M$  is the moment arm with respect to the pivot point  $O$  and  $N$  is the total number of discrete points.

To compute the flow field within the cell interior, velocity boundary conditions were applied along the cell membrane. The cell membrane was assumed to be in quasistatic equilibrium, and the pivot point of the membrane rotational motion was approximated to be the projection point of the cell center of gravity on the substrate

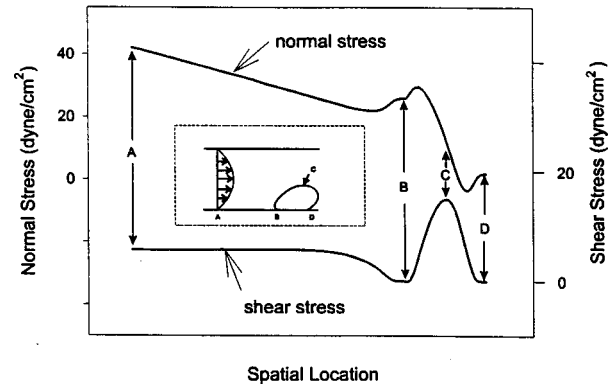


**FIGURE 5.** Distribution of the normal and tangential shear stresses along a deformed cell surface within a  $30 \mu\text{m}$  diam vessel (wall shear stress  $\tau_w=6.0 \text{ dyn/cm}^2$ ). The spatial locations A-B-C-D along the abscissa correspond to the actual sites (inset) along the wall and the cell surface.

[Fig. 2(a)]. To better represent the flow close to the moving boundary, three layers of elements with specified depths [Fig. 3(b)] were attached around the cell membrane prior to an automatic meshing for the remaining computational domain of the cell interior with a total of 1344 element nodes [Fig. 3(b)]. The actual fluid shear stress and normal stress acting on the cell inner surface were computed coupling with cell deformation.

## RESULTS

In the present cell adhesion and deformation model, a cell diameter of  $8 \mu\text{m}$  and a vessel channel height ( $2D$ ) of  $30 \mu\text{m}$  were assumed. Both intracellular and extracellular flow fields for an adherent cell under shear are illustrated in Figs. 3(c) and 3(d). Using the parameters listed in Table 1 for this model, Fig. 4(a) shows the calculated 2D cell shapes in a shear flow, where a WBC is adherent to the EC under a fluid wall shear stress ( $\tau_w$ ) of  $6.0 \text{ dyn/cm}^2$ . The cellular cytoplasmic viscosity ( $\mu_c$ ) of the adherent WBC was predicted to be around 100 P, which was derived from the best agreement between the experimentally measured and the computed indices in cell shapes (e.g.,  $L_c$ ,  $H_c$ , and  $W_c$ ; Fig. 2) at various time points [e.g.,  $t_0$ ,  $t_p$  and  $t_e$ ; Figs. 1(a)–1(c)]. Time  $t=t_0$  ( $t_0=0^+$  s) represents the instant at which a WBC just attaches to the EC and quickly deforms into an initial teardrop shape. Time  $t=t_p$  (e.g.,  $t_p=3.8$  s, under  $\tau_w=6.0 \text{ dyn/cm}^2$ ) is the time point that the WBC initiates detachment from the EC. After time  $t_p$ , the cell starts a peeling process while the trailing edge of the WBC membrane moves in the direction of the blood flow. The actual distance of the cell movement from time  $t_p$  to  $t_e$  was computed [Fig. 4(a)]. Figure 4(b) shows the com-

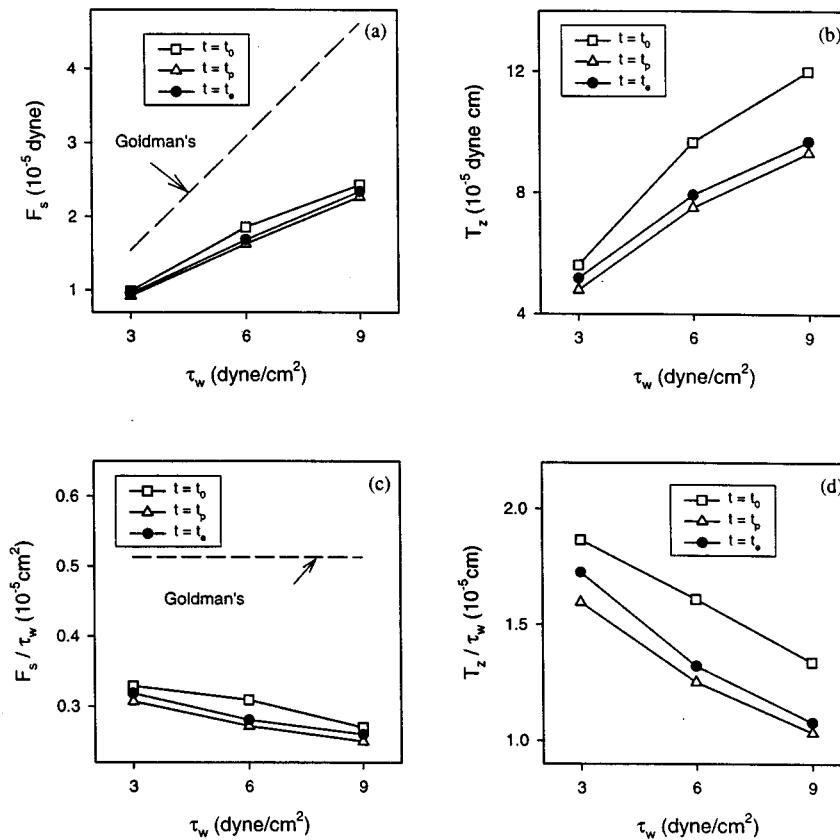


FIGURE 6. Computed results: (a) horizontal drag force  $F_s$ ; (b) torque  $T_z$ ; and (c), (d) drag coefficients  $F_s/\tau_w$  and  $T_z/\tau_w$ , respectively, on a single cell adhered to the venular wall (vessel diameter = 30  $\mu\text{m}$ ) as a function of wall shear stress  $\tau_w$ . The different time instants represent different cell shapes with deformation. Goldman's curves represent results from a rigid sphere under the same flow conditions described.

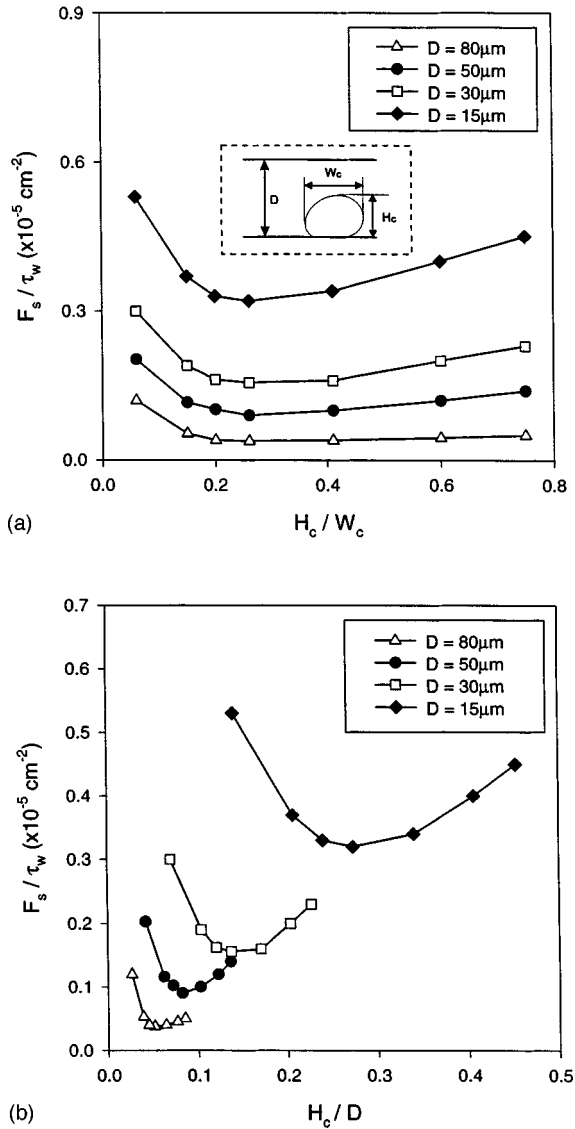
puted cell-shape changes under different wall shear stresses (e.g.,  $\tau_w = 3.0, 6.0,$  and  $9.0$  dyn/cm<sup>2</sup>) at time  $t = t_p$ .

Figure 5 shows that the actual shear stress around the cell is very different from the inlet wall shear stress  $\tau_w$ . For example, shear stress  $\tau$  starts at  $\tau = \tau_w = 6.0$  dyn/cm<sup>2</sup> away from a cell (point A) and is gradually reduced in its magnitude as flow approaches the cell (point B). The shear stress then rapidly increases along the deformed cell surface as the vessel lumen becomes more obstructed by the cell. The peak stress (point C) was found to be  $\tau_{\text{max}} = 2.5 \tau_w$  in a range of inlet wall shear stress 3.0–9.0 dyn/cm<sup>2</sup>. The shear stress drops as the vessel lumen widens again along the leading surface of the cell (point D). This stress resumes its upstream value at some point downstream. The pressure drop across one cell (e.g., in a 30  $\mu\text{m}$  vessel channel) was found to be around  $\Delta p = 14$ –45 dyn/cm<sup>2</sup> at  $\tau_w$  of 3.0–9.0 dyn/cm<sup>2</sup>.

The horizontal drag force ( $F_s$ ) and torque ( $T_z$ ) on a WBC were calculated as a function of  $\tau_w$  as shown in Figs. 6(a) and 6(b). While both  $F_s$  and  $T_z$  increase as  $\tau_w$  becomes larger [Figs. 6(a) and 6(b)], the ratios of  $F_s/\tau_w$  and  $T_z/\tau_w$  decrease when  $\tau_w$  increases [Figs. 6(c) and 6(d)], suggesting that the fluid drag force and torque acting on an individual cell increase disproportionately

less than  $\tau_w$ , most likely due to cell deformation. Figure 6 also shows that  $F_s$ ,  $T_z$ ,  $F_s/\tau_w$ , and  $T_z/\tau_w$  all have the largest value at time  $t_0$  (cells are less deformed) and the smallest value at  $t_p$  (cells are more deformed) for any given  $\tau_w$ . If it is assumed that the cell is a rigid sphere in close proximity to the substrate, the drag force  $F_s$  or  $F_s/\tau_w$  may be estimated from the formulation of Goldman, *et al.*<sup>15</sup> As illustrated in Figs. 6(a) and 6(c), the solution of Goldman and co-workers yields much greater values for  $F_s$  and  $F_s/\tau_w$ . These results demonstrate how cell-shape changes or cell deformability may affect the total fluid drag force and torque on the adherent cells in a shear flow. It is these fluid forces that are transmitted via a deformable cell body to the cell–surface contact region, which generate a peeling force that breaks the adhesive bonds.

Figure 7 further elucidates the relationships among the fluid drag coefficient  $F_s/\tau_w$ , the vessel channel height  $D$ , and cell dimension. The computations reveal that  $F_s/\tau_w$  increases as  $D$  decreases [Fig. 7(a)]. The influence of WBC deformation (characterized by cell-shape index  $H_c/W_c$ ) on  $F_s/\tau_w$  becomes more apparent when  $D$  is small (e.g.,  $D < 15 \mu\text{m}$ ).  $F_s/\tau_w$  decreases as  $H_c/W_c$  decreases from 0.8 to 0.4 for a given  $D$  under a wall shear stress 6 dyn/cm<sup>2</sup> [Fig. 7(a)]. With further reductions in  $H_c/W_c$ , a minimum value of  $F_s/\tau_w$  is



**FIGURE 7.** Fluid drag coefficient on a deformed cell affected by: (a) cell deformation represented by a ratio of cell height  $H_c$  to the cell projection length  $W_c$  ( $D$  is the channel height for a 2D vessel); and (b) vessel lumen obstruction by a cell characterized by a ratio of  $H_c/D$ .

attained when  $H_c/W_c$  approaches 0.2, following which  $F_s/\tau_w$  increases with further reductions in  $H_c/W_c$ .

The total adhesive force resulting from the receptor–ligand bonds depends on the bond density [ $N_b$ ; Eqs. (12) and (13)]. Such a force is a function of both time and the peeling tension that is acting on each bond [Eqs. (7)–(9)]. The bond kinetic change would alter the bond distribution and the WBC–EC surface contact gap  $Y(X)$  (Fig. 2), hence, change the total adhesive strength to resist the flow-induced peeling forces. Figure 8(a) shows the nondimensional peeling gap  $Y/L_b$  between the WBC and EC surfaces as a function of a peeling distance  $X/L_b$  ( $0 \leq X < \delta$ ).  $L_b$  is the length for a unstretched bond

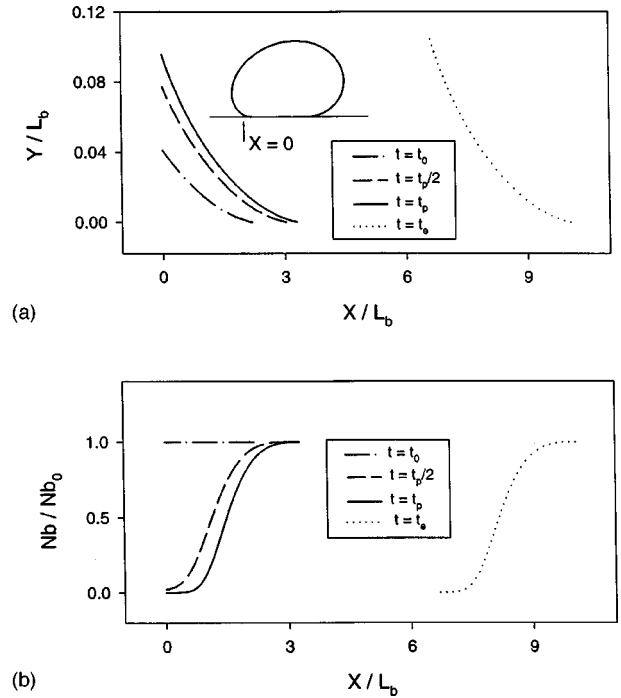


**FIGURE 8.** Theoretical predictions on (a) WBC–EC peeling gaps ( $Y$ ) as a function of both space ( $X$ ) and time ( $t$ ). Wall shear stress is  $3.0 \text{ dyn/cm}^2$ .  $L_b$  is the unstretched bond length ( $L_b = 50 \text{ nm}$ ). The inset defines  $X=0$  location. (b) Spatial and temporal distributions of receptor–ligand bond density ( $N_b$ ).  $N_{b0}$  is the initial bound density ( $N_{b0} = 1.3 \times 10^{10} \text{ dyn/cm}^2$ ).

and  $\delta$  is the active peeling zone within the total contact region of  $L_c$  (Fig. 2). The results were calculated under  $\tau_w = 3.0 \text{ dyn/cm}^2$  at four different time points  $t = t_0$ ,  $t_p/2$ ,  $t_p$ , and  $t_e$ , respectively. These gaps  $Y(X)$  represent the different extent at which each individual bond is stressed under the tensile-peeling forces from the cell membrane. The peeling gap increases as time increases from  $t_0$  to  $t_p$ . It is noticed from the experimental observation (Fig. 1) that the entire frame of the WBC membrane begins to move in the direction of flow after time  $t_p$ , analogous to a rigid body rotation about the WBC center. The total distance moved by a cell was predicted by multiplying the average peeling velocity ( $V_p$ ) with the time difference of  $\Delta t = t_e - t_p$  as shown in Figs. 4(a) and 8(a). Within the same peeling zone  $\delta$ , the actual bond density distributions ( $N_b$ ) corresponding to the gaps shown in Fig. 8(a) were also predicted from the present cell adhesion model [Fig. 8(b)]. From Fig. 8(b), it can be seen that there is a significant drop in bond density at time  $t = t_p/2$  and  $t_p$ , which suggests a mode of temporal dependence on bond density based on the kinetic Eq. (7)–(9). This drop becomes more apparent especially near the trailing edge [ $X=0$ ; Fig. 2(c)], where the largest peeling forces are exerted on the receptor–ligand bonds. To obtain these results, an initial bond density ( $N_{b0}$ ) was as-

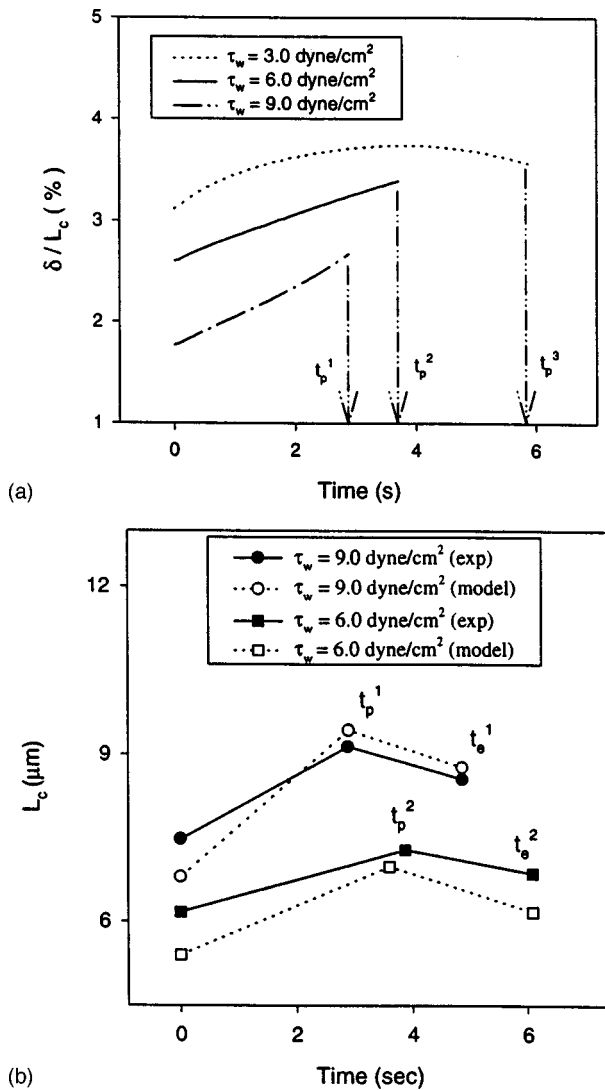


**FIGURE 9.** (a) Ratios of active peeling zone ( $\delta$ ) to the total contact length ( $L_c$ ) as a function of time.  $\tau_w$  is the wall shear stress and  $t_p$ 's are the different peeling times (superscripts 1–3 on  $t_p$  are for  $\tau_w=9.0, 6.0$ , and  $3.0$  dyn/cm<sup>2</sup>, respectively). (b) Comparison of the results obtained from the experimental measurements and theoretical predictions on WBC-EC contact length  $L_c$ .

sumed to be uniformly distributed at time  $t=t_0$  within the area of WBC-EC contact. Based on the kinetic model proposed by Bell,<sup>3</sup> it was also assumed that the time needed (from  $t=0$  to  $t=t_0=0^+$  s) to form a bond would be very short compared with the scale of the adhesion time  $t_p$ . The bond density  $N_{b0}$ , therefore, represents the total equilibrium in bond formation within a “zero” time period.  $N_{b0}$ , however, depends on the initial density of total receptors  $N_r$  on the WBC and ligands  $N_l$  on the EC, as well as the kinetic rate constants  $K_+$  and  $K_-^0$  [Eqs. (8) and (9)].

The ratio of the active membrane peeling length ( $\delta$ ) to the entire contact length ( $L_c$ ) was computed from time  $t_0$

to  $t_p$ , under wall shear stresses ranging from 3.0 to 9.0 dyn/cm<sup>2</sup>. Figure 9(a) shows that only a very small portion of the entire cell-surface contact ( $\delta/L_c \sim 2\% - 4\%$ ) is actually under the tensile peeling force. It is this small peeling zone  $\delta$  that provides all the adhesive-bond forces to resist the fluid-induced drag force. Under higher shear stresses (e.g.,  $\tau_w=6.0$  or  $9.0$  dyn/cm<sup>2</sup>), the  $\delta/L_c$  ratio increases with time due to a fact that  $\delta$  increases more than that in  $L_c$ . This suggests that a cell is actively being detached from its substrate faster than the cell can be deformed by the shear force. In contrast, the  $\delta/L_c$  ratio shows a biphasic change with time under a low shear stress (e.g.,  $\tau_w=3.0$  dyn/cm<sup>2</sup>), in which the  $\delta/L_c$  ratio increases during an initial time period followed by a subsequent decrease at a later time. Obviously, a decrease in the  $\delta/L_c$  ratio indicates that  $L_c$  increases disproportionately more than  $\delta$  under low shear stresses, in which cell deformation becomes more apparent than cell-surface detachment. The model predictions on the WBC-EC contact length  $L_c$  were directly compared with experimental measurements (e.g., Fig. 1) as a function of time for different wall shear stresses [Fig. 9(b)]. The parameters used to calculate  $L_c$  are tabulated in Table 1. The cytoplasmic viscosity and cell membrane bending stiffness were estimated to be around 100 P and  $1.5 \times 10^{-9}$  ergs, respectively. Figure 9(b) illustrates that an increase in wall shear stress results in an increase in WBC-EC contact length  $L_c$ , but a decrease in peeling time  $t_p$ .

The relative influence of both cytoplasmic viscosity and membrane bending stiffness on the overall cell deformability were examined. Figure 10(a) shows how cell deformation at an onset time  $t_0$  responds to a 10- to 20-fold increase in cytoplasmic viscosity under a given wall shear stress ( $\tau_w=6.0$  dyn/cm<sup>2</sup>). The cytoplasmic viscosity  $\mu_c$  significantly influences cell-surface contact as well in terms of  $\delta/L_c$  [Fig. 10(d)]. To characterize the effect of membrane elasticity on the cell-shape change and cell-surface contact, changes in membrane bending stiffness  $B$  were tested for a given wall shear stress [Figs. 10(b) and 10(c)]. These results demonstrate the sensitivity of the cell deformation to alterations in the membrane bending stiffness of the WBC cortical layer.

The influence of cell receptor density  $N_r$  and substrate ligand density  $N_l$  on the peeling time  $t_p$  was characterized for different cell deformations as shown in Fig. 11, where  $\beta$  is an index of the cell-shape changes that reflects the ratios of cell height and width at two different times:  $t_p$  and  $t_0$  (i.e.,  $\beta = \{H_c/W_c\}_{t_p} / \{H_c/W_c\}_{t_0}$ ). Given a cell shape, e.g., from Fig. 4(a) ( $\beta \approx 0.8$ ,  $N_r = 3.0 \times 10^{10}$  mol/cm<sup>2</sup>),  $t_p$  changes as a function of  $N_l$  [Fig. 11(a)]. A nearly linear relationship between  $t_p$  and  $N_l$  was found for low values of  $N_l$ . As shown from Fig. 11(a), there is a critical value of  $N_l$  ( $\sim 1.0 \times 10^9$  mol/cm<sup>2</sup>) below which  $t_p$  apparently approaches zero,

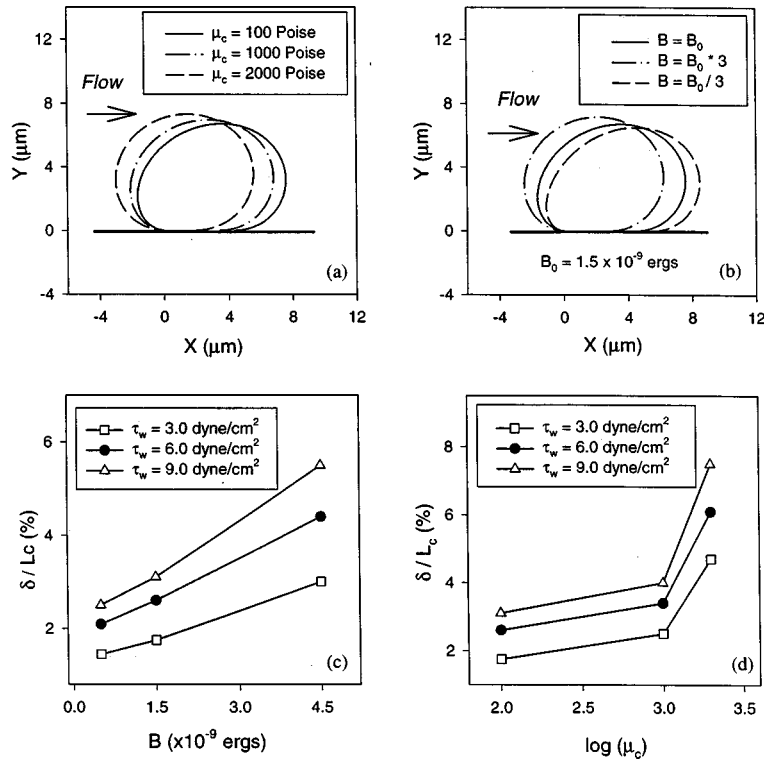


**FIGURE 10.** Influence of cytoplasmic viscosity ( $\mu_c$ ) and cortical layer bending stiffness ( $B$ ) on cell shapes (a) and (b) and cell-surface contact (c) and (d) at the time of initial attachment ( $t_0$ ). Wall shear stress  $\tau_w = 6.0$  dyn/cm<sup>2</sup>. (a) and (d): Change in cytoplasmic viscosity  $\mu_c$  (with  $B = 1.5 \times 10^{-9}$  ergs). (b) and (c): Change in membrane bending stiffness  $B$  (with  $\mu_c = 100$  P;  $B_0 = 1.5 \times 10^{-9}$  ergs).

indicating that cells cannot maintain adherence to the substrate under the given flow shear stress. The current calculations also suggest that the critical values of ligand density [minimal values in Fig. 11(a)] for maintaining cell adhesion ( $t_p > 0$ ) are not significantly influenced by cell deformation or wall shear stress. However, a greater value in ligand density will result in a longer peeling time  $t_p$ . When a cell becomes stiffer (e.g.,  $\beta \approx 1.0$ ), the peeling time  $t_p$  will become shorter than those for deformable cells (e.g.,  $\beta \approx 0.6$ ). The sensitivity of the peeling time to receptor density  $N_r$  [Fig. 11(b)] appears to increase as the ligand density increases. Figure 11(c) illustrates the effects of bond kinetics [characterized by  $F_{rs} = \{K_s - K_{ts}\}/K_s$ ; Eqs. (8) and (9)] on the transient adhesion in terms of  $t_p$ . Results from Fig. 11 suggest that the cell-surface adhesion time is predominately affected by the receptor-ligand bond density and kinetics in contrast to the extent of cell deformation.

## DISCUSSION

Numerical calculations have been presented to investigate the mechanics of WBC deformation and adhesion to the EC in shear flow and to elucidate the effect of cellular mechanical properties on the equilibrium between hydrodynamic and adhesive forces.

Both *in vivo* measurements (Fig. 1) and numerical simulation (Fig. 4) have shown that under a given wall shear stress, the contact length  $L_c$  increases with time as

new bonds are formed at the leading edge.  $L_c$  then decreases with time as the trailing edge of the WBC membrane peels away from the EC [bond breakage was assumed to occur at  $S=0$ ; Fig. 2(c)]. The time  $t_p$  was found to decrease if the wall shear stress  $\tau_w$  increased. A significant linear correlation ( $p < 0.05$ ) between  $\ln(t_p)$  and  $\tau_w$  was previously found by Struble *et al.*<sup>25</sup> in which they showed a logarithmic decline of  $t_p$  with  $\tau_w$ . Their study suggested that  $t_p$  could be equivalent to the bond lifetime under a given separation force, which would be consistent with the kinetic theory of fracture developed by Zhurkov<sup>30</sup> and Bell.<sup>3</sup> The present study has used time  $t_p$  to characterize the transient state of WBC-EC adhesion at which the cell starts to peel away from the substrate during the initiation of WBC-EC separation.

The relationship between wall shear stress along the EC and peak shear stress on the WBC surface was calculated. The shear stress at the highest point of a cell (point C in Fig. 5) was found to be 2.5 times of the upstream wall shear stress ranging from 3.0 to 9.0 dyn/cm<sup>2</sup>. However, such an estimate based on a 2D model could fall short in an actual 3D flow field. For example, Cao *et al.*<sup>4</sup> found the maximum shear stress on an adherent cell surface in a 3D flow field would be almost 4.0 times of the inlet wall shear stress. Similar shear stress distributions were also observed in other studies of low Reynolds number flow over spreading cells,<sup>22</sup> although less rigorous estimates of shear stress on the WBC surface were made. The pressure drop across

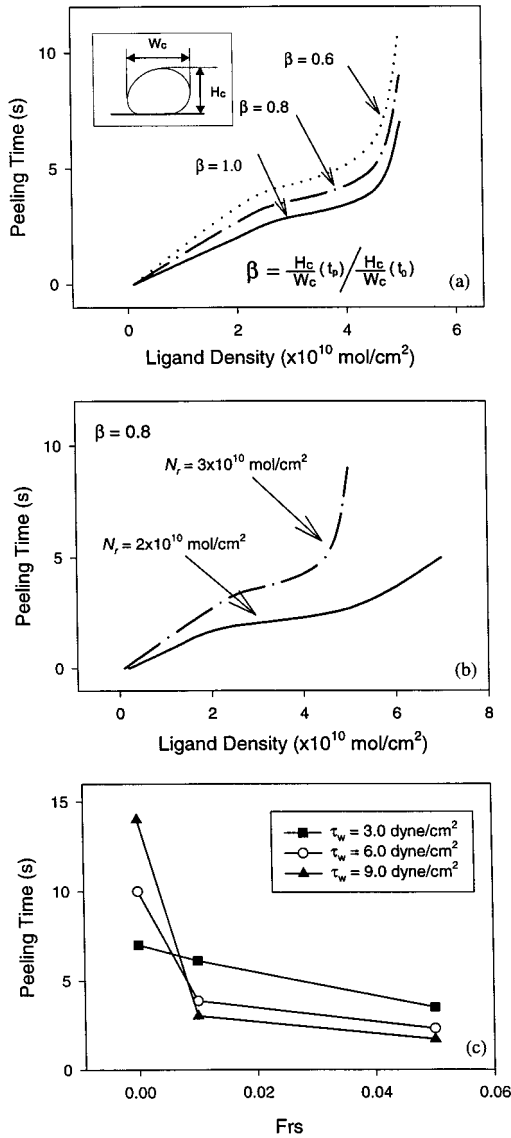


**FIGURE 11.** Changes of the peeling time  $t_p$  as a function of the EC ligand density  $N_l$  (a) and (b) and bond constant  $K_{ts}$  (c).  $\beta$  is the ratio of  $H_c/W_c(t_p)$  and  $H_c/W_c(t_0)$  characterizing the cell deformability.  $H_c$  is the cell height and  $W_c$  is the cell projection length.  $N_r$  is the WBC receptor density. Wall shear stress is  $6.0$  dyn/cm<sup>2</sup> for (a) and (b). (a) Influence of  $N_l$  on  $t_p$  with different  $\beta$  ( $N_r = 3.0 \times 10^{10}$  mol/cm<sup>2</sup>). (b) Influence of  $N_r$  on  $t_p$  with different  $N_l$  ( $\beta = 0.8$ ). (c) Influence of  $K_{ts}$   $\{F_{rs} = (K_s - K_{ts})/K_s\}$  on  $t_p$  under different wall shear stresses ( $N_r = N_l = 3.0 \times 10^{10}$  mol/cm<sup>2</sup>,  $K_s = 4.0$  dyn/cm).

one cell is found to be around  $14.0$ – $45.0$  dyn/cm<sup>2</sup> for  $\tau_w$  of  $3.0$ – $9.0$  dyn/cm<sup>2</sup>, which is within the range of experimental conditions. A pressure drop across an adherent cell was previously reported by House and Lipowsky<sup>18</sup> from an actual *in vivo* measurement to be about  $40$  dyn/cm<sup>2</sup> under a similar flow condition.

The influence of cell deformation on the total horizontal force  $F_s$  and torque  $T_z$  on the cell has been char-

acterized.  $F_s$  and  $T_z$  were calculated from time  $t_0$  to  $t_e$  (Fig. 6) by integrating the total fluid stresses acting on a deformed 2D ring with an effective ring width of  $6 \mu\text{m}$  [Fig. 2(a)]. For a given wall shear stress  $\tau_w = 6.0$  dyn/cm<sup>2</sup>, Fig. 6(a) shows that  $F_s$  decreases from time  $t_0$  to  $t_p$  due to an increase in cell deformation [Fig. 4(a)]. The computed force  $F_s$  on a deformable cell ranges from  $1.3$  to  $2.3 \times 10^{-5}$  dyn under wall shear stresses  $\tau_w = 3.0$ – $9.0$  dyn/cm<sup>2</sup>, which is significantly smaller than that on a rigid sphere calculated by the method of Goldman *et al.*<sup>15</sup> Schmid-Schönbein *et al.*<sup>23</sup> estimated that a drag force between a leukocyte and the endothelium was in an order ranging from  $4.0 \times 10^{-6}$  to  $23.4 \times 10^{-5}$  dyn as determined from *in vitro* models. House and Lipowsky<sup>18</sup> also calculated the leukocyte–endothelium adhesion force ranging from  $1.1$  to  $76.1 \times 10^{-5}$  dyn with a mean force of  $12.1 \times 10^{-5}$  dyn based upon *in vivo* measurements of pressure drop along the venular wall. It has been found that the force  $F_s$  and torque  $T_z$  both increase [Figs. 6(a) and 6(b)] with an increase in wall shear stress within the range that we have tested ( $\tau_w = 3.0$ – $9.0$  dyn/cm<sup>2</sup>). In contrast, the drag coefficient  $F_s/\tau_w$  or  $T_z/\tau_w$ , for a deformable cell decreases as  $\tau_w$  increases [Figs. 6(c) and 6(d)], suggesting that the drag acting on an individual WBC increases disproportionately less than  $\tau_w$  due to cell deformation. The current calculations on the drag [Fig. 6(c)] agree with those earlier experiments on *in vivo* force determination.<sup>18</sup> The magnitude of  $F_s/\tau_w$ , however, is somewhat different from that of House and Lipowsky,<sup>18</sup> where values of  $F_s/\tau_w$  decreased from  $1.5 \times 10^{-5}$  to  $0.25 \times 10^{-5}$  dyn as  $\tau_w$  increased from  $2.0$  to  $6.0$  dyn/cm<sup>2</sup> within a  $35 \mu\text{m}$  diam vessel. The greater *in vivo* values may be attributed to the increased stiffness of the *in vivo* WBCs (which protruded further into the lumen) attained during adhesion stimulated by the chemoattractant fMLP. Irregularities in the microvessel wall and hence a departure from a circular cross section may also be a factor contributing to this disparity.

To further elucidate the mechanics of WBC–EC adhesion and deformation in a small vessel, the relationships among the fluid drag coefficient  $F_s/\tau_w$ , the vessel channel height  $D$ , and cell dimension were examined (Fig. 7). It has been found that  $F_s/\tau_w$  decreases as  $H_c/W_c$  decreases from  $0.8$  to  $0.4$  for a given  $D$  and a wall shear stress [Fig. 7(a)]. When  $H_c/W_c$  approaches  $0.2$ , a minimum value of  $F_s/\tau_w$  is attained following which  $F_s/\tau_w$  increases with further reductions in  $H_c/W_c$ . In that extreme situation, it would be possible that any slight decrease in cell height ( $H_c$ ) may cause an increase in cell projection length ( $W_c$ ) due to the cell volume conservation. As a result, an additional increase in fluid–cell surface contact area will possibly increase the horizontal fluid drag force on a very deformed cell. Figure 7(b) further illustrates the extent to which the

fluid drag force is influenced by ratios of the cell height to the channel height (i.e.,  $H_c/D$ ). The reversed trend of  $F_s/\tau_w$  dependence on cell deformation is strongly affected by the vessel dimensions. While these results are qualitatively similar to the simple ‘‘pill box’’ model of House and Lipowsky,<sup>18</sup> they offer greater detail and presumably a more realistic appraisal of the role that cell deformation plays in affecting the drag force on an adherent WBC.

The fluid drag forces acting upon a WBC will be transmitted to forces that disrupt individual adhesive bonds between WBC and EC. Both  $F_s$  and  $T_z$  are balanced by adhesive forces, which are influenced by the bond elastic constant  $K_{ts}$ , the bond density  $N_b$ , the active WBC–EC separation area  $A_c$  (characterized by the peeling length  $\delta$ ), the location of a mass center, and the bond tilting angle  $\theta$  [Fig. 2(c)]. It is evident from the present calculations which represent incipient WBC rolling that the peeling gap  $Y=Y(X)$  and the peeling distance  $X=\delta$  change as a function of time and location [Fig. 8(a)]. This behavior results in both temporal and spatial changes in  $N_b$  [Fig. 8(b)], and hence the bond force  $f_x=A_c N_b f_b \sin(\theta+\phi)$ . Because of the temporal change in  $N_b$  under a given wall shear stress  $\tau_w$ , an adherent cell in a shear flow deforms as a function of time in order to readjust the force balance ( $F_s=f_x$ ) to maintain its adherence to the EC (Fig. 4). As the peeling gap  $Y=Y(X)$  continuously increases [Fig. 8(a)] and bond density  $N_b$  decreases with time [ $t_0 < t < t_p$ ; Fig. 8(b)], a final equilibrium state must be reached at which the bonds at the trailing edge of the WBC–EC contact [point  $P_c$  in Fig. 2(c)] reach a critical density  $N_{bc}$ . The time needed to reach this critical point has been characterized in the present study by the peeling time  $t_p$ , subsequent to which the cell initiates movement ( $t_p < t < t_e$ ). The distance of a curve shifting due to the cell detachment from its substrate was determined from the experimental measurements (Fig. 1). The average bond tilting angles were predicted to be around  $45.5^\circ$ – $65.0^\circ$  from the calculations for a shear stress ranging from 3.0 to 9.0 dyn/cm<sup>2</sup>. This prediction is close to the angle of  $55.5^\circ$  estimated by Alon *et al.*<sup>1</sup> in their studies of the lifetime of the *P*-selection carbohydrate bond under a shear stress of 1.1 dyn/cm<sup>2</sup>.

The active peeling distance  $\delta$  has been found to be less than 5% of the total contact  $L_c$  and depends on the wall shear stress, adhesion time, and cell deformation [Fig. 9(a)]. The  $\delta$  zone may also depend on the mechanical properties of cell membrane and bond adhesion strength.<sup>5,11</sup> It should be noted that the computed and measured values of  $L_c$  are in close agreement. Some differences between calculation and experiment [Fig. 8(b)] may also arise from artifacts in the *in vivo* images,<sup>28</sup> which may result from out-of-focus information. The apparent WBC–EC contact length also depends

strongly on the intercellular viscosity  $\mu_c$  and cell membrane bending stiffness  $B$ .

Both cytoplasmic viscosity [Fig. 10(a)] and cell membrane elasticity [Fig. 10(b)] have a profound influence on cell deformation. For red blood cells, there is very little extension in cell surface area during cell deformation. RBC deformability is predominated by the bending and shearing rigidity of the cell membrane. Membrane (or thin shell) theory is usually adequate to describe the rheological behavior of the WBC cortical layer without considering the bending property<sup>7–9,13</sup> because of a large amount of surface folds. Comparing with the RBC membrane bending stiffness of  $10^{-12}$  ergs,<sup>10</sup> a WBC bending modulus in an order of  $10^{-11}$  erg was recently reported by Zhelev *et al.*<sup>29</sup> from a micropipette measurement on a suspended white cell under static deformation. Also, a bending stiffness of  $2.0 \times 10^{-9}$  ergs was estimated by Olivier and Truskey<sup>22</sup> in calculating the fluid on a spreading cell in a laminar flow using a parallel-plate flow chamber. The current 2D model shows that such a membrane bending rigidity ( $B$ ) has a significant influence on cell deformation [Fig. 10(b) and 10(c)]. Figure 10(c) (an adherent cell under a shear force) suggests a general parametric trend that  $\delta/L_c$ , a ratio between the active peeling zone  $\delta$  and the total contact length  $L_c$ , would decrease when  $B$  becomes smaller. For example,  $\delta/L_c$  is about 3%–6% (depending on shear stresses) when  $B$  is in an order of  $10^{-9}$  erg.  $\delta/L_c$  decrease to approximately 1%–2% when  $B$  values are less than  $10^{-10}$  erg, indicating that a ‘‘softer’’ cell membrane would result in larger cell deformation with an increase in cell–surface contact length  $L_c$ . We have further found that the total contact length  $L_c$  increases disproportional more than those of the active peeling zone  $\delta$  when  $B$  decreases. Cell deformation is also sensitive to cytoplasmic viscosity  $\mu_c$  [Fig. 10(a)]. Figure 10(d) indicates a general parametric trend that  $\delta/L_c$  would increase from 1%–3% to 5%–8% when  $\mu_c$  increases from  $10^2$  to  $10^3$  P, indicating that a more viscous core in cell cytoplasm would result in smaller cell deformation with a decrease in cell–surface contact length  $L_c$ . We found that the total contact length  $L_c$  decreases disproportional more than those of the active peeling zone  $\delta$  when  $\mu_c$  increases. Although some discrepancies might exist in estimating  $\mu_c$  and  $B$  for a WBC,<sup>13,22,29</sup> it would be noted that most parameters are very ‘‘apparent,’’ depending on a model (2D or 3D). Those apparent parameters also depend on an actual experimental assay (a suspended cell under static condition or an adherent cell on a flat surface subject to a shear flow). The apparent parameters obtained in this study were derived from the best agreement with the *in vivo* experimental measurements on cell shapes, cell–surface contact length  $L_c$  ( $\delta$  could not be measured), transient adhesion time  $t_p$ , and various shear stresses. Without concluding what should be an ‘‘appropriate’’ magnitude

for  $\mu_c$  and  $B$ , a general parametric trend shown in Fig. 10 has provided an important insight showing how WBC rheological properties would affect cell deformation, hence, the cell–surface adhesion.

The relative influence of cell-shape changes and ligand density  $N_l$  on the peeling time  $t_p$  was characterized for a wall shear stress of 6 dyn/cm<sup>2</sup>. Shown in Fig. 11(a), an extremely high  $N_l$  will result in an infinite long  $t_p$ , indicating that the present shear stress may not be high enough to detach the WBC from the EC. In contrast, if  $N_l$  becomes extremely low,  $t_p$  will be close to zero, which implies that cells cannot maintain adherence to the endothelium. As shown in Fig. 11(a), cell deformability has less significant influence on the peeling time. On the other hand, given an EC ligand density on the substrate, the surface receptor density  $N_r$  on a WBC can also change the WBC–EC peeling time [Fig. 11(b)]. With the current 2D model, a bond lifetime was characterized by a measurable time constant  $t_p$  regulated by a parameter  $K_{ts}$  [Eq. (9)]. Dembo *et al.*<sup>5</sup> defined a bond as a “slip bond” if  $K_{ts} < K_s$ ; while they called an “ideal bond” when  $K_{ts} = K_s$ . Results from Fig. 11(c) predict that the smaller  $K_{ts}$  is ( $F_{rs} = \{K_s - K_{ts}\}/K_s$ ), the shorter the peeling time  $t_p$  (transient adhesion) will be. An “ideal bond” would have a longer adhesion time. Since  $K_{ts}$  affects the bond density  $N_b$  [Eqs. (7)–(9)], the number of bonds is very sensitive to the formation of a “stable adhesion” ( $t_0 < t < t_p$ ) and an initiation of cell rolling ( $t_p < t < t_e$ ).

Although a 2D model has its limitations on an estimate of forces, time, and other results in describing the actual 3D situation, the present model provides a useful means to characterize the influence of cellular deformability on the transient cell adhesion processes. Among all those parameters, the fluid shear stress  $\tau_w$  has the most significant impact on almost all solutions, such as cell shapes [Fig. 4(b)], drag forces (Fig. 6), cell–surface contact interface [Fig. 9(a); Figs. 10(c) and 10(d)], and transient adhesion [Fig. 9(b); Fig. 11(c)]. Rheological parameters, such as cell membrane bending modulus  $B$  and cytoplasmic viscosity  $\mu_c$ , have profound effects on cell shapes [Figs. 10(a) and 10(b)] and the cell–surface contact interface [Figs. 10(c) and 10(d)]. Flow channel dimension  $D$  appears to affect drag forces (Fig. 7). Adhesion receptor ( $N_r$ ) or ligand ( $N_l$ ) densities and bond property (characterized by  $K_{ts}$  in  $F_{rs}$ ) seem to have more influence on adhesion time [Figs. 11(b) and 11(c)] than that for cell shapes [Fig. 11(a)]. In general, a more deformable cell would be less easy to detach because of a smaller drag force (Fig. 6). Recent work by Lei *et al.*<sup>20</sup> also showed that a less deformable cell would roll faster due to less energy dissipation from both cell cytoplasm and cell–surface adhesion.

In summary, the analyses presented in this paper allow us to understand the basic mechanics of leukocyte deformation and adhesion to the vascular endothelium in shear flow. Beyond the parametric studies presented here, the major conclusion is that the transmission of shear forces to the entire cortical shell of the WBC and their resultant action on a relatively small “peeling zone” at the cell’s trailing edge is a process that cannot be ignored or overly simplified, if one is to obtain meaningful descriptions of *in vivo* events. It is apparent that much further experimental and theoretical studies are needed to fully elucidate the mechanics of WBC–EC adhesion.

## ACKNOWLEDGMENTS

This study was supported in part by a Whitaker Foundation research grant and NSF Career Award No. BES-9302079 (C.D.), and grants from PHS, Grant Nos. HL-28381 and HL-39286 (H.H.L.).

## REFERENCES

- Alon, R., D. A. Hammer, and T. A. Springer. Lifetime of the P-selectin–carbohydrate bond and its response to tensile force in hydrodynamic flow. *Nature (London)* 374:539–542, 1995.
- Baker, M., and H. Wayland. On-line volume flow rate and velocity profile measurement for blood in microvessels. *Microvasc. Res.* 7:131–143, 1974.
- Bell, G. I. Models for the specific adhesion of cells to cells. *Science* 200:618–627, 1978.
- Cao, J., B. Donnell, D. R. Deaver, M. B. Lawrence, and C. Dong. *In vitro* side-view imaging technique and analysis of human T-leukemic cell adhesion to ICAM-1 in shear flow. *Microvasc. Res.* 55:124–137, 1998.
- Dembo, M., D. C. Torney, K. Saxman, and D. A. Hammer. The reaction-limited kinetics of membrane-to-surface adhesion and detachment. *Proc. R. Soc. London* 234:55–83, 1988.
- Dembo, M. On peeling an adherent cell from a surface. *Lect. Math. Life Sci.* 24:51–77, 1994.
- Dong, C., R. Skalak, K.-L. P. Sung, G. W. Schmid-Schönbein, and S. Chien. Passive deformation analysis of human leukocytes. *J. Biomech. Eng.* 110:27–36, 1988.
- Dong, C., R. Skalak, and K.-L. P. Sung. Cytoplasmic rheology of passive neutrophils. *Biorheology* 28:557–567, 1991.
- Dong, C., and R. Skalak. Leukocyte deformability: Finite element modeling of large viscoelastic deformation. *J. Theor. Biol.* 158:173–193, 1992.
- Evans, E. Minimum energy analysis of membrane deformation applied to pipet aspiration and surface adhesion of red blood cells. *Biophys. J.* 30:265–284, 1980.
- Evans, E. Detailed mechanics of membrane–membrane adhesion and separation, I. Continuum of molecular cross-bridges. *Biophys. J.* 48:175–183, 1985.
- Evans, E., and R. Skalak. *Mechanics and Thermodynamics of Biomembranes*. Boca Raton, FL: CRC, 1980, pp. 101–117.
- Evans, E., and A. Yeung. Apparent viscosity and cortical tension of blood granulocytes determined by micropipet aspiration. *Biophys. J.* 56:151–160, 1989.

- <sup>14</sup>Firrell, J. C., and H. H. Lipowsky. Leukocyte margination and deformation in mesenteric venules of rat. *Am. J. Physiol.* 256:H1667–1674, 1989.
- <sup>15</sup>Goldman, A. J., R. G. Cox, and H. Brenner. Slow viscous motion of a sphere parallel to a plane wall II—Couette flow. *Chem. Eng. Sci.* 22:653–660, 1967.
- <sup>16</sup>Hammer, D. A., and S. M. Apte. Simulation of cell rolling and adhesion on surfaces in shear flow: General results and analysis of selectin-mediated neutrophil adhesion. *Biophys. J.* 63:35–57, 1992.
- <sup>17</sup>Hammer, D. A., and D. A. Lauffenburger. A dynamical model for receptor-mediated cell adhesion to surfaces. *Biophys. J.* 52:475–487, 1987.
- <sup>18</sup>House, S. D., and H. H. Lipowsky. *In vivo* determination of the force of leukocyte–endothelium adhesion in the mesenteric microvasculature of the cat. *Circ. Res.* 63:658–668, 1988.
- <sup>19</sup>Lawrence, M. B., and T. A. Springer. Leukocytes roll on a selectin at physiologic flow rates: Distinction from and prerequisite for adhesion through integrins. *Cell* 65:859–873, 1991.
- <sup>20</sup>Lei, X., M. B. Lawrence, and C. Dong. Influence of cell deformation on leukocyte rolling adhesion in shear flow. *J. Biomech. Eng.* (in review).
- <sup>21</sup>Lipowsky, H. H., D. Rigel, and G. S. Shi. *In vivo* mechanical properties of leukocytes during adhesion to venular endothelium. *Biorheology* 28:53–64, 1991.
- <sup>22</sup>Olivier, L. A., and G. A. Truskey. A numerical analysis of forces exerted by laminar flow on spreading cells in a parallel plate flow chamber assay. *Biotechnol. Bioeng.* 42:963–973, 1993.
- <sup>23</sup>Schmid-Shönbein, G. W., Y. C. Fung, and B. W. Zweifach. Vascular endothelium–leukocyte interaction, sticking shear force in venules. *Circ. Res.* 36:173–184, 1975.
- <sup>24</sup>Springer, T. A. Traffic signals for lymphocyte recirculation and leukocyte emigration: The multistep paradigm. *Cell* 76:301–314, 1994.
- <sup>25</sup>Struble, E. J., C. Dong, and H. H. Lipowsky. Leukocyte deformation and endothelial cell contact mechanics during incipient membrane peeling and cell rolling. *FASEB J.* 7:A903, 1993.
- <sup>26</sup>Tözeren, A., K.-L. Sung, and S. Chien. Theoretical and experimental studies on cross-bridge migration during cell disaggregation. *Biophys. J.* 55:479–487, 1989.
- <sup>27</sup>Ward, M. D., M. Dembo, and D. A. Hammer. Kinetics of cell detachment: Effect of ligand density. *Ann. Biomed. Eng.* 23:322–331, 1995.
- <sup>28</sup>Zhe, S., and H. H. Lipowsky. Image enhancement of the *in vivo* leukocyte–endothelium contact zone using optical sectioning microscopy. *Ann. Biomed. Eng.* 25:521–535, 1996.
- <sup>29</sup>Zhelev, D. V., D. Needham, and R. M. Hochmuth. Role of the membrane cortex in neutrophil deformation in small pipets. *Biophys. J.* 67:696–705, 1994.
- <sup>30</sup>Zhurkov, S. N. Kinetic concept of the strength of solids. *Int. J. Fract. Mech.* 1:311–323, 1965.